CHAPTER 3

Compact Filtering Antenna with High Selectivity and Improved Performance for L-band Applications

3.1 Introduction

The wireless communication system has been experiencing a revolutionary growth in the last few decades. This growth has been caused due to the invention of many wireless products and services including global positioning system (GPS), mobile communication, satellite communication and amateur radio operations. In these systems, the size of both antennas and filters designed using first principles is comparable to the wavelength of the signal. The components designed in this way would be of large physical size for the desired applications and hence need was felt to miniaturize the conventionally designed antennas. Keeping this aspect in view, various types of antennas [Lai and Luk (2008), Sharma *et al*. (2015), Joshi and Singhal (2018), Lee *et al*. (1999), Liang *et al*. (2005), Liu *et al*. (2011), Liu *et al*. (2013), Goswami and Karia (2017)] have been investigated. Among these antennas, planar monopole antennas (MPAs) of different shapes viz rectangular, circular, and elliptical shapes [Lee *et al*. (1999), Liang *et al*. (2005), Liu *et al*. (2011), Liu *et al*. (2013), Goswami and Karia (2017)] have been of particular research interest because of their compact size, simple structure, wide frequency impedance bandwidth, easy fabrication and omnidirectional radiation patterns. But, these antennas have some drawbacks, such as poor band-edge selectivity and the presence of unwanted harmonics. Due to these drawbacks, chances of unwanted frequency components being received by the antennas cannot be ruled out. This would affect the performance of systems using these antennas. Hence, an antenna

of this type is usually followed by a suitable bandpass filter (BPF) to improve its performance over the frequency band of operation and to suppress unwanted harmonics.

To improve the signal-to-noise ratio (S/N) performance of a receiver used for the aforesaid applications, it is imperative to place low noise amplifier (LNA), which includes BPF in its circuit, in close proximity with the antenna by reducing the length of the transmission line connecting the antenna to LNA. That provided the researchers with a purpose to integrate the filter and antenna into a single compact component, known as filtering antenna that performs filtering and radiation functions simultaneously. Various types of filtering antennas are available in the literature [Abbaspour-Tamijani *et al*. (2002), Zuo *et al*. (2009), Mandal and Chen (2010), Wu *et al*. (2013), Cheng and Li (2017), Wu *et al*. (2011), Mansour *et al*. (2014)]. In [Zuo *et al*. (2009)], integrated design of antenna and filter is reported which share same ground plane to achieve compact co-design of the filter-antenna system. The cascaded approach used to design antenna-filter systems is reported in [Mandal and Chen (2010), Wu *et al*. (2013), Cheng and Li (2017)]. In [Wu *et al*. (2011), Mansour *et al*. (2014)], a resonator of the filter structure is replaced by a radiating element to obtain compact filtering antenna providing desirable filtering and radiation characteristics.

The reported filtering antennas required improvement in terms of size and/or filtering and radiation performance.

In this chapter, a new compact L-band filtering antenna having sharp cut-off performance and reasonably suppressed unwanted harmonics is presented. The filtering antenna is obtained through integration of a modified elliptic-shaped MPA with the modified interdigital bandpass filter (IBPF) presented in **chapter 2**. The BPF is responsible for obtaining improved cut-off performance in the desired frequency band with good suppression of unwanted harmonics. In the initial phase, a modified elliptic-

shaped MPA was designed and investigated through numerical simulation and measurement. Further, the modified IBPF presented in chapter 2 is integrated with the proposed antenna to achieve compact integrated system having good impedance matching within the desired passband, improved band-edge selectivity and wide stopband with reasonably suppressed out-of-band unwanted harmonics. The proposed integrated system will henceforth be referred to as filtering antenna. The proposed MPA and the proposed filtering antenna are studied through numerical simulation and measurement. The numerical simulation study is carried out using Ansys high-frequency structure simulator (HFSS) numerical simulation software based on the finite element method (FEM). Roger RT/duroid 6010 substrate (ε_r = 10.2, tanδ = 0.0023, thickness = 1.27 mm) was used for design, simulation and experimental studies of the proposed monopole antenna and the proposed filtering antenna.

3.2 Proposed Modified Elliptic-shaped Monopole Antenna(MPA)

3.2.1 Design and Investigation of the Proposed Antenna

The geometrical configuration of the proposed modified elliptic-shaped MPA along with its shape parameters is shown in Figure 3.2(a). The proposed MPA is evolved from a conventional circular-shaped MPA. The design stages involved in the evolution of the proposed antenna from a conventional circular-shaped MPA is shown in Figure 3.1. Figure 3.1 shows the geometries of five shapes of MPA along with the proposed modified elliptic-shaped MPA. Circular-shaped MPAs having a partial rectangular ground plane and modified partial ground plane have been designated as ‘Type-I’ and ‘Type-II’ antennas respectively, whereas elliptic-shaped MPAs having a partial rectangular ground plane and modified partial ground plane have been designated as ‘Type-III’ and ‘Type-IV’ antennas respectively. ‘Type-V’ antenna consists of a

modified elliptic-shaped patch which is a combination of two modified elliptic-shaped patches and partial rectangular ground plane. Roger RT/duroid 6010 substrate material (ε_r = 10.2, tanδ = 0.0023, thickness = 1.27mm) is used for design of all MPAs along with the proposed antenna. The proposed antenna consists of a modified elliptic-shaped patch and modified ground plane fed through a 50 Ω microstrip line with a tapered transition. The top side of the proposed antenna consists of a combination of two modified elliptic-shaped patches connected to 50 Ω microstrip feedline through a tapered transition. The modified elliptic-shaped patch is responsible for increasing the electrical length of the proposed antenna which shifts its resonant frequency to lower side without increasing its physical size, thereby making the antenna more compact. The bottom side of the proposed antenna contains a modified ground plane having curved shape and a rectangular notch in the central region of its upper side. The rectangular notch helps in efficiently tuning the mutual coupling between the radiating element and the ground over a wide frequency range. The curved shape in the upper region of the ground plane is introduced for smooth transition from one resonant mode to another across wide bandwidth which ensures good impedance matching over a wide frequency range. The values of optimized geometrical parameters of the proposed antenna are given in Table 3.1. The overall size of the proposed antenna is 78.8 mm × 47 mm × 1.27 mm. The basic shapes of MPA along with the proposed antenna have been designed and numerically simulated in order to compare their reflection coefficient-frequency characteristics. For a fair comparison, the physical size of all the antennas including the proposed antenna is kept the same.

In order to understand the operating mechanisms of various types of MPA structures along with the proposed one, the current distributions on the surfaces of these antenna configurations are discussed. Figure 3.3 depicts the surface current distributions

for various types of MPA configurations at the frequencies of 1, 1.8, and 2.6 GHz. From Figure 3.3, it can be observed that more or equivalent current is concentrated on the surface of the proposed antenna as compared to other antenna configurations at different frequencies of interest. Hence, it can be said that the proposed antenna configuration is properly excited to provide better performance as compared to other investigated antenna configurations.

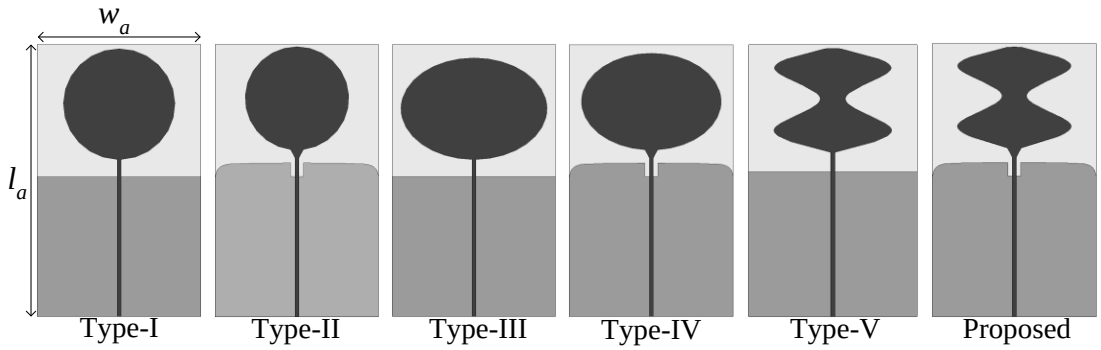

Figure 3.1: Geometries of different monopole antennas: circular-shaped with partial rectangular ground plane (Type-I), circular-shaped with modified partial ground plane (Type-II), elliptic-shaped with partial rectangular ground plane (Type-III), elliptic-shaped with modified partial ground plane (Type-IV), modified elliptic-shaped with partial rectangular ground plane (Type-V), and modified elliptic-shaped with modified partial ground plane (proposed antenna).

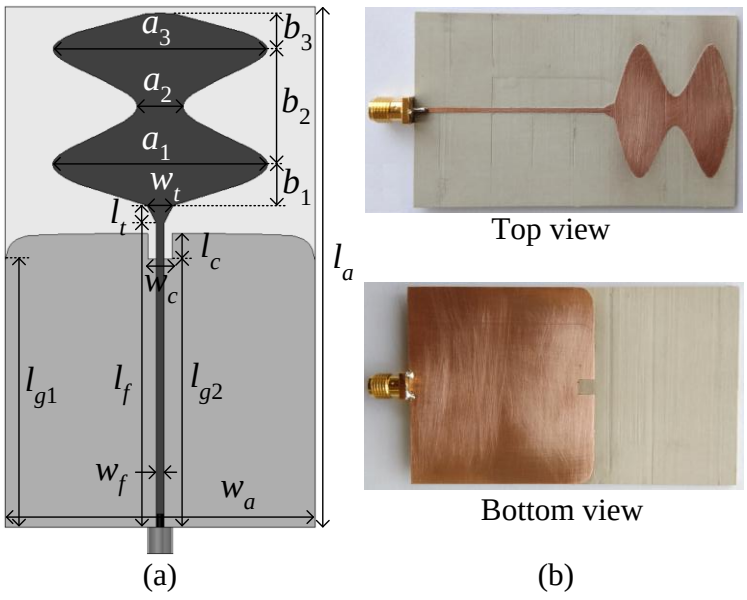

Figure 3.2: (a) Geometry of the proposed modified elliptic-shaped monopole antenna. (b) Top and bottom views of the fabricated prototype of the proposed modified elliptic-shaped monopole antenna.

Table 3.1: Optimized geometrical parameter values of the proposed antenna (all dimensions are in millimeter).

l_a = 78.8	w_a = 47	l_f = 46	w_f = 1.1	l_c = 3.9	w_c = 3.7	l_t = 2.7	w_t = 4
l_{g1} = 40.5	l_{g2} = 40.6	a_1 = 32.6	a_2 = 7	a_3 = 32.5	b_1 = 6.2	b_2 = 17.4	b_3 = 5.5

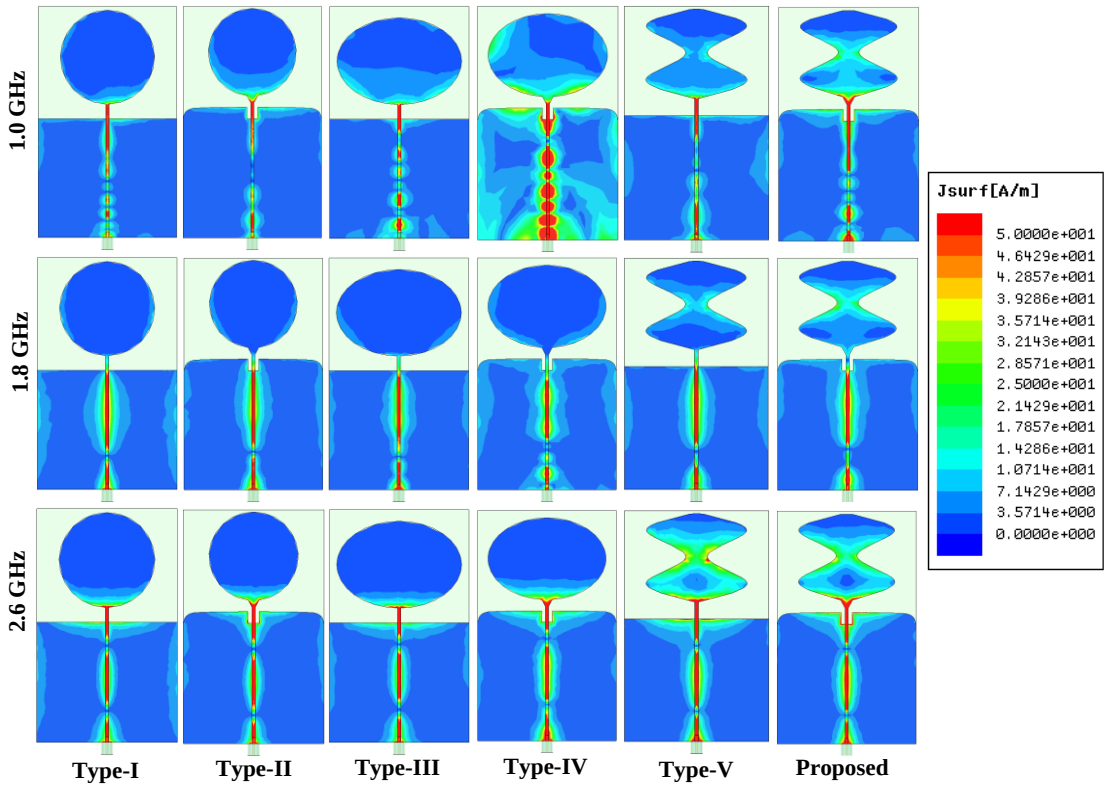

Figure 3.3: Simulated surface current distributions for different geometries (Type-I, Type-II, Type-III, Type-IV, Type-V and Proposed) of the monopole antennas at the frequencies of 1.0, 1.8, and 2.6 GHz.

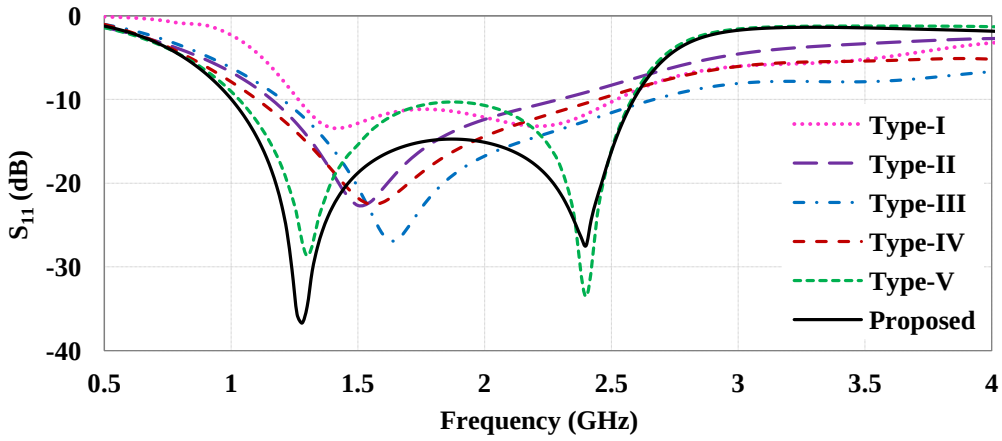

Figure 3.4: Numerically simulated variations of reflection coefficient with frequency for different geometries (Type-I, Type-II, Type-III, Type-IV, Type-V and Proposed) of the monopole antennas.

Figure 3.4 shows the simulated variations of reflection coefficient with frequency for six different geometries of the antenna, which include 'Type-I', 'Type-II', 'Type-III', 'Type-IV', 'Type-V', and the proposed antennas. The objective of present investigation is to design and develop a compact antenna which covers wide frequency range with good impedance matching. To achieve that objective, initially conventional circular-shaped antenna is chosen and through step-by-step modification in the geometry, the proposed compact antenna configuration is obtained finally which provides good impedance matching over a wide frequency range. With the antenna of Type I/II/III/IV/V, difficulty is faced in obtaining good impedance matching over wide frequency range without compromising the compactness of the antenna structure. That is why, further modification is done in the geometry to obtain the configuration of the proposed compact MPA, which provides good impedance matching over wide frequency range (1.0 – 2.6 GHz). To clearly show the differences in characteristics of different types of MPAs, reflection coefficient versus frequency plots of these antennas are shown in Figure 3.4 up to 4 GHz. Table 3.2 shows the comparative study in terms of impedance bandwidth for the same physical area of various types of monopole antennas shown in Figure 3.1. From Figure 3.4 and Table 3.2, it can be easily observed that the proposed compact MPA provides the widest -10 dB reflection coefficient bandwidth of 88.9% in the frequency range 1.0 – 2.6 GHz along with good impedance matching over the desired frequency range.

Further, the proposed MPA is numerically simulated for its radiation patterns, realized gain-frequency characteristic, and total efficiency-frequency characteristic in addition to its input characteristic. Furthermore, the prototype of the proposed antenna was fabricated using printed circuit board (PCB) Technology for experimental study in order to validate the simulation results for antenna's input characteristics, radiation

patterns and realized gain-frequency characteristics. Figure 3.2(b) shows the top and bottom views of the fabricated prototype of the proposed modified elliptic-shaped MPA. A sub-miniature version A (SMA) connector was used for feeding microwave power to the antenna through the microstrip line as shown in Figure 3.2(b).

Table 3.2: Comparison of various types of monopole antennas in terms of bandwidth and physical area.

Monopole antenna type	**Impedance bandwidth**
Type-I	1.26 GHz (1.27 – 2.53 GHz)
Type-II	1.11 GHz (1.17 – 2.28 GHz)
Type-III	1.45 GHz (1.21 – 2.66 GHz)
Type-IV	1.33 GHz (1.11 – 2.44 GHz)
Type-V	1.53 GHz (1.04 – 2.57 GHz)
Proposed	1.6 GHz (1.0 – 2.6 GHz)

*The physical area of all types of monopole antennas is same (= 78.8 mm × 47 mm).

3.2.2 Results and Discussion

3.2.2.1 Reflection Coefficient-Frequency Characteristics

Figure 3.5 shows numerically simulated and measured variations of reflection coefficient of the proposed MPA with frequency. From Figure 3.5, it can be observed that the simulated -10 dB reflection coefficient bandwidth of the proposed antenna covers the frequency range 1.0 – 2.6 GHz. It can also be observed from Figure 3.5 that around the simulated frequency of 5.7 GHz, unwanted harmonics are present. Because of the presence of unwanted harmonics, signal interference occurs in a communication system and it affects the S/N performance of the receiver circuitry. Hence, in order to achieve a better S/N performance of receiver circuitry in a wireless communication system, out-of-band harmonics should be suppressed. The magnitudes of reflection coefficient of the proposed antenna were measured using Anritsu make vector network analyser (VNA) Master (Model: MS2038C). The measured -10 dB reflection coefficient

bandwidth of the proposed antenna covers the frequency range of 1.01 – 2.50 GHz. It can be seen from Figure 3.5 that the simulated and measured results are nearly in agreement with each other excepting minor variations over the frequency range of interest due to fabrication tolerances and measurement errors.

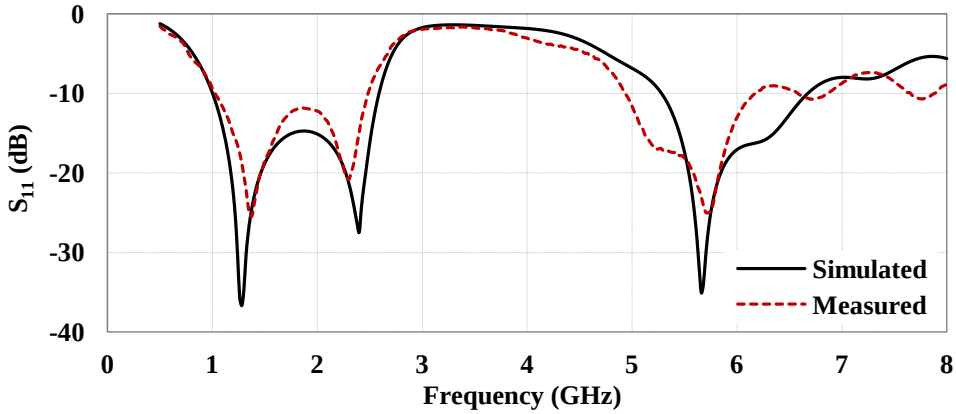

Figure 3.5: Numerically simulated and measured variations of reflection coefficient of the proposed antenna with frequency.

3.2.2.2 Radiation Patterns and Peak Realized Gain-Frequency Characteristics

The simulated and measured co- and cross-polarized radiation pattern plots of the proposed antenna in E- and H-planes for three different frequencies (1.1, 1.8, 2.5 GHz) are presented in Figure 3.6. From Figure 3.6, it can be observed that the proposed antenna exhibits good omnidirectional co-polar radiation patterns with low cross-polarization levels at the frequencies of interest. The cross-polarization levels in E-plane are found to be less as compared to the corresponding levels in H-plane at a given frequency.

Figure 3.7 shows the simulated and measured realized gain values of the proposed antenna with frequency. The simulated (measured) realized gain values vary in the range 2.2 – 3.5 dB (1.9 – 3.3 dB) over the operating frequency range of 1.0 – 2.6 GHz (1.01 – 2.50 GHz).

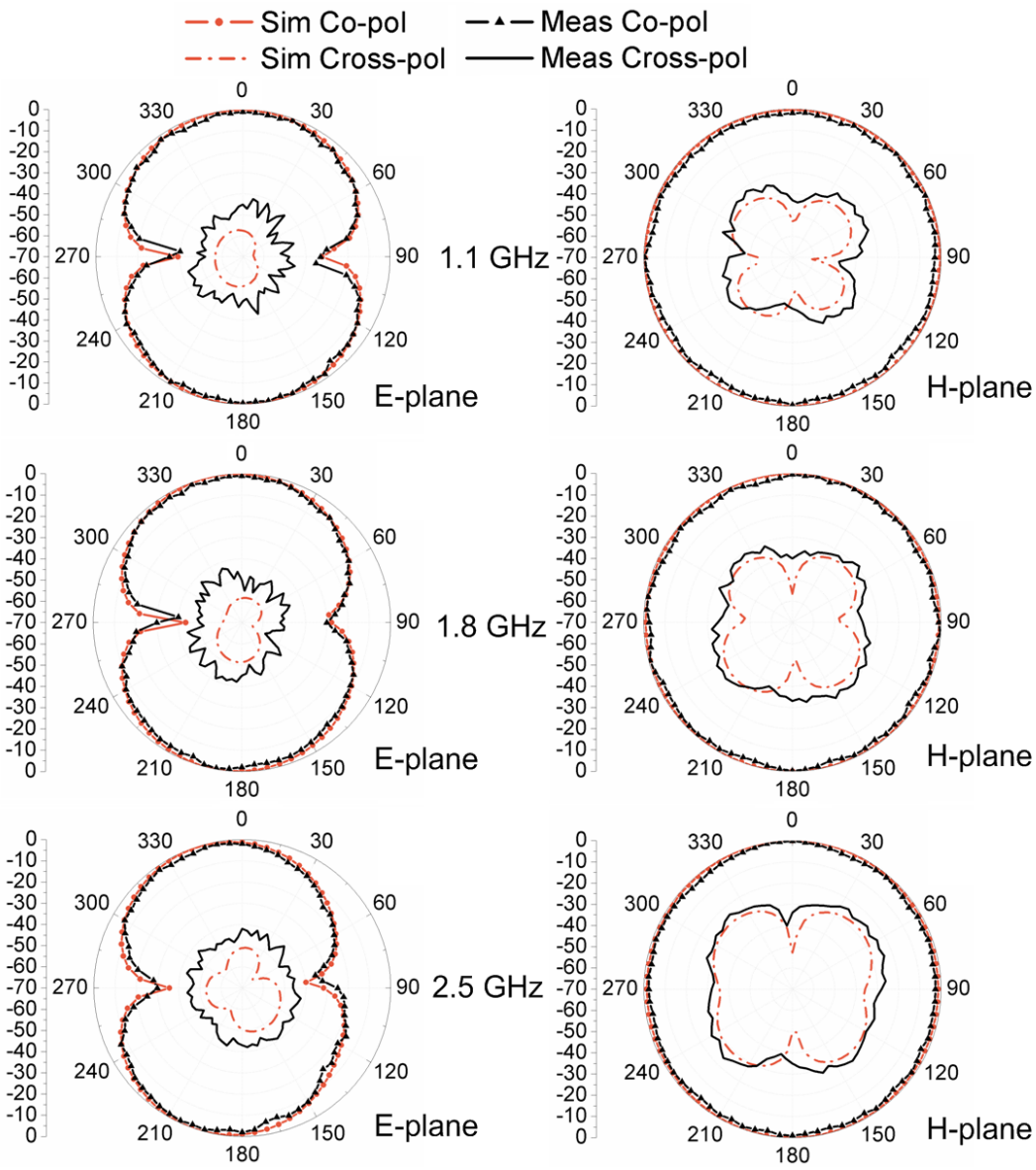

Figure 3.6: Numerically simulated and measured radiation patterns of the proposed antenna for three different frequencies of 1.1, 1.8, 2.5 GHz.

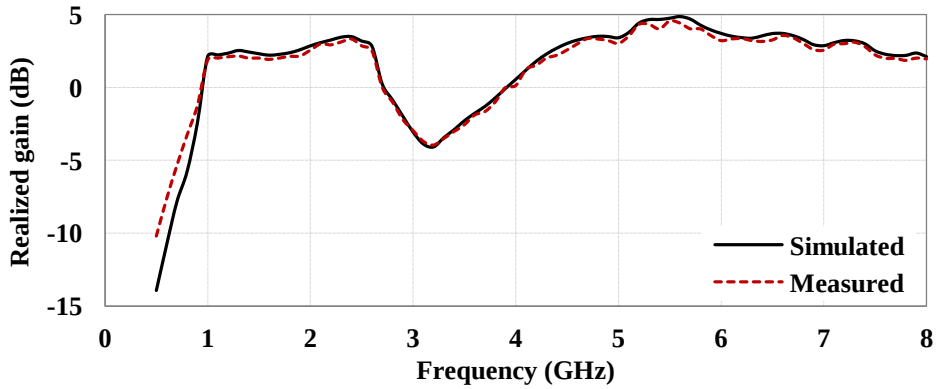

Figure 3.7: Numerically simulated and measured gain values of the proposed antenna as functions of frequency.

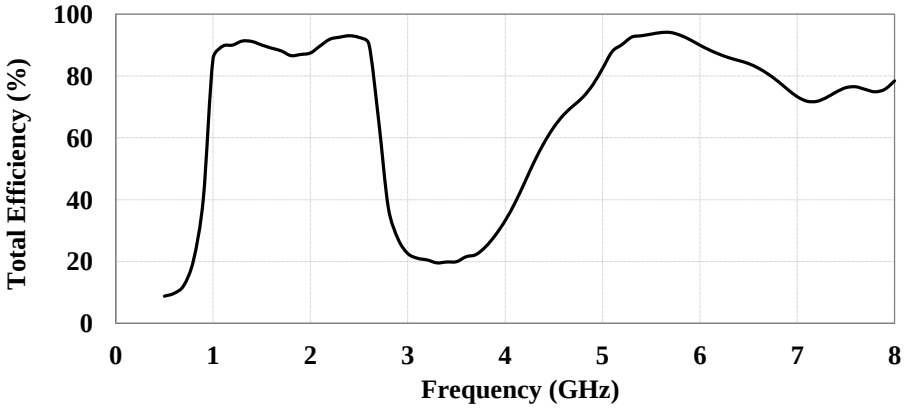

Figure 3.8: Simulated total efficiency of the proposed antenna as function of frequency.

3.2.2.3 Simulated Total Efficiency-Frequency Characteristic

Figure 3.8 shows the simulated variation of total efficiency of the proposed antenna with frequency. From the Figure 3.8, it can be observed that values of total efficiency vary over the range 86 – 93 % in the desired passband 1.0 – 2.6 GHz. In the undesired frequency range, the total efficiency initially decreases but starts increasing from 3.3 GHz and peaks at 5.7 GHz, where its value reaches ~ 94 %. Thereafter, it shows decreasing trend up to 7.2 GHz and finally more or less increasing trend in the frequency range of 7.2 – 8.0 GHz.

3.2.2.4 Performance Comparison of the Proposed Antenna with Those Reported in Literature

Further, the dimension based comparison of the proposed MPA with those reported in the literature is provided in Table 3.3. It is apparent from Table 3.3 that overall electrical size of the proposed antenna (in terms of wavelength, λ_l) is smaller than the sizes of antennas reported in the literature. The proposed antenna provides almost stable radiation patterns with reasonably good realized gain values over its operating frequency band. However, the proposed antenna needs improvement in terms of cut-off performance in order to improve band-edge selectivity in the desired passband

frequency range and unwanted harmonic suppression in the out-of-band frequency range.

Table 3.3: Comparison of the proposed monopole antenna with the antennas reported in the literature.

Reference	Lower cut-off frequency, f_l (GHz)	Physical size (mm × mm)	Electrical size ($\lambda_l \times \lambda_l$)
[Liang *et al*. (2005)]	2.69	50 × 42	0.448 × 0.376
[Liu *et al*. (2011)]	1.02	110 × 124	0.374 × 0.42
[Liu *et al*. (2013)]	1.05	80 × 74	0.28 × 0.259
[Goswami and Karia (2017)]	2.8	55.9 × 33	0.52 × 0.308
Proposed antenna	**1.01**	**78.8 × 47**	**0.265 × 0.16**

λ_l is the free space wavelength at the lower cut-off frequency (f_l).

3.3 The Modified Interdigital Bandpass Filter (IBPF)

3.3.1 Design of the Modified IBPF

In order to achieve sharp cut-off performance and wide stopband with reasonably suppressed out-of-band unwanted harmonics of the proposed MPA, the modified IBPF presented in **chapter 2** is used. The modified IBPF is effectively integrated with the proposed MPA in order to obtain an L-band filtering antenna for applications in L-band wireless communication. It is to be noted that certain design principles were considered during the integration of the BPF with the antenna. First, the dielectric substrate employed for the BPF should be same as that used for the antenna. Second, the characteristic impedance of the microstrip line feeds at the input and output ports of the filter must be equal to 50 Ω i.e. the microstrip line width at the input and output ports of the filter should meet 50 Ω impedance criterion. Third, the -10 dB reflection coefficient bandwidth of the filter should cover the L-band frequency range in order to achieve the L-band filtering antenna. The dielectric substrate, RT/duroid 6010, having dielectric

constant of 10.2 and thickness of 1.27 mm was used for design. Figure 3.9(a) shows the perspective view of the modified IBPF having spurlines and defected ground structures (DGSs). Figures 3.9(b) and 3.9(c) show the top and bottom views of the BPF. The detailed design procedure of the BPF is available in chapter 2. The geometrical parameter values of the BPF for L-band operation are given in Table 3.4. The size of the compact BPF is 20.2 mm × 9.0 mm × 1.27 mm.

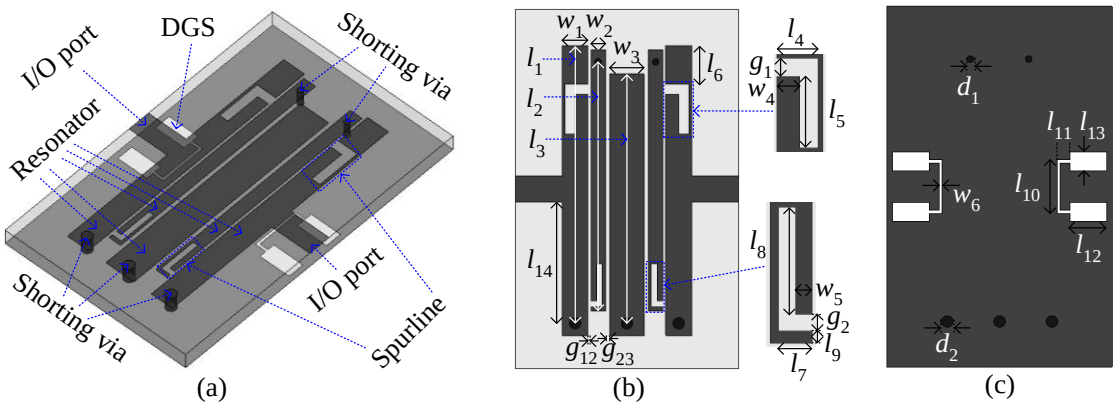

Figure 3.9: Geometry of the BPF (a) Perspective view, (b) Top view, and (c) Bottom view.

Table 3.4: Geometrical parameter values of the BPF (all dimensions are in millimetre)

l_1 = 19.3	w_1 = 1.8	l_2 = 17.3	w_2 = 1	l_3 = 17.2	w_3 = 2.4	g_{12} = 0.2
g_{23} = 0.3	d_1 = 0.4	d_2 = 0.8	l_4 = 1.6	l_5 = 2.8	l_6 = 2.7	g_1 = 0.7
w_4 = 0.9	l_7 = 0.8	l_8 = 2.6	l_9 = 0.3	g_2 = 0.4	w_5 = 0.4	l_{10} = 3.7
l_{11} = 0.9	l_{12} = 2.5	l_{13} = 1.3	w_6 = 0.2	l_{14} = 8.4		

3.3.2 Results and Discussion

The simulated variations of the magnitude of *S*-parameters of the BPF with frequency are shown in Figure 3.10. From Figure 3.10, it can be observed that -10 dB reflection coefficient bandwidth of the BPF is 1.05 GHz (= 71.6 %) and covers the frequency range 0.94 – 1.99 GHz. The 3-dB passband frequency range of the BPF is 0.89 – 2.05 GHz. As far as the stopband performance of the BPF is concerned, the upper stopband

attenuation level is better than 17 dB up to 8 GHz. The maximum value of simulated insertion loss at a mid-band frequency of the filter passband is found to be 0.35 dB.

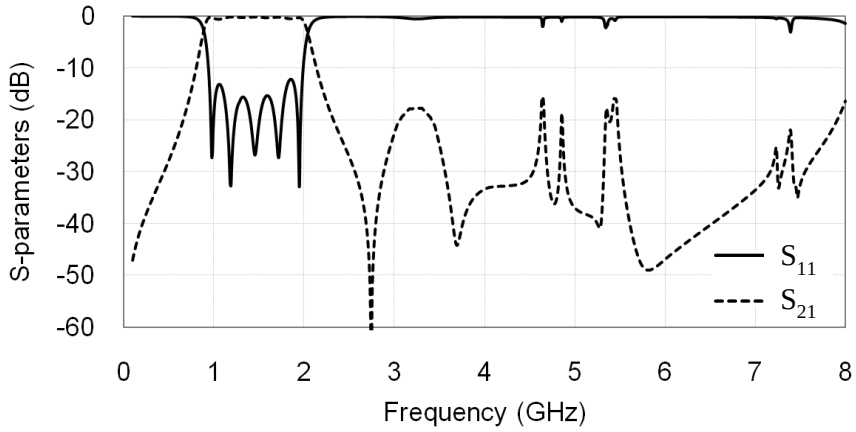

Figure 3.10: Numerically simulated variations of the magnitude of *S*-parameters of the BPF versus frequency.

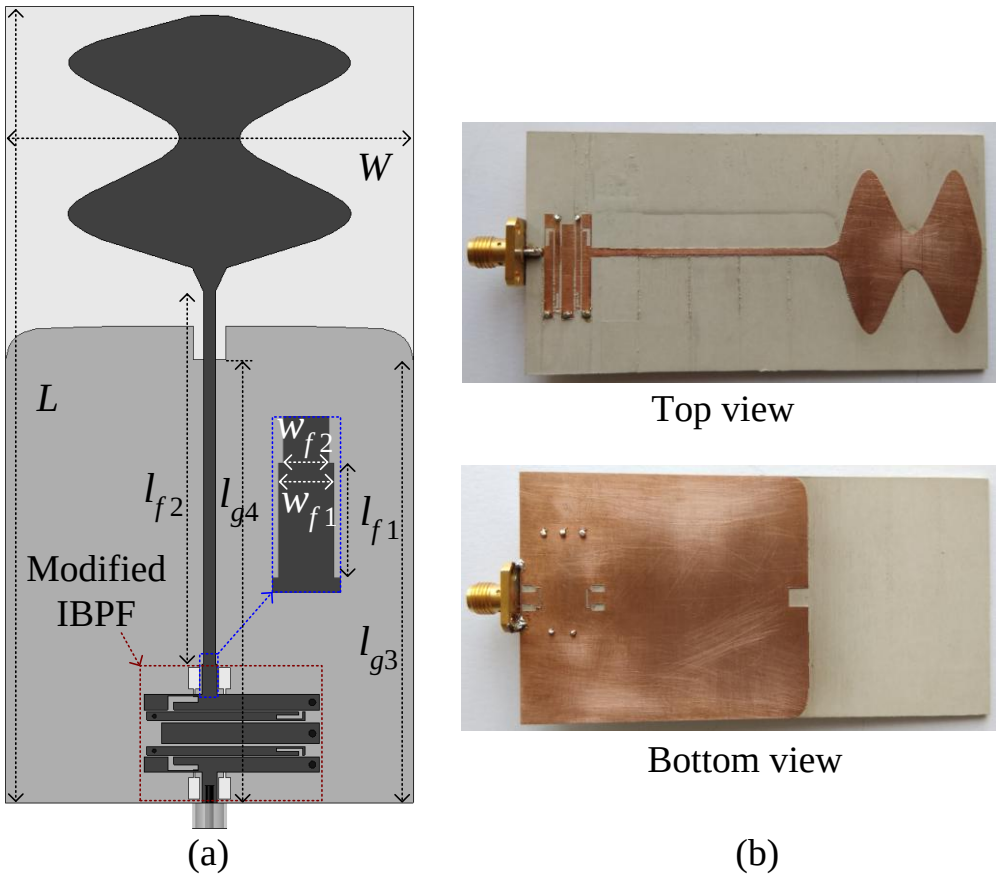

Figure 3.11: (a) Geometry of the proposed integrated design of filtering antenna. (b) Top and bottom views of the fabricated prototype of the proposed integrated design of filtering antenna.

3.4 Proposed Filtering Antenna

3.4.1 Design and Investigation of the Proposed Filtering Antenna

The modified elliptic-shaped MPA is integrated with the modified IBPF to obtain the proposed L-band filtering antenna having sharp passband cut-off performance and reasonably suppressed out-of-band unwanted harmonics so that it can find potential application in a compact L-band wireless communication system. The L-band integrated system/component is designed due to various advantages and applications of L-band frequency range (1 – 2 GHz). The GPS signals are used in L-band of frequency spectrum because L-band wave can penetrate clouds, fog, rain, storm and vegetation, and it requires less expensive hardware and smaller size components/system. L-band is also used for satellite communication, mobile communication, and aircraft surveillance. Figure 3.11(a) shows the geometry of the proposed filtering antenna, obtained through integration of modified elliptic-shaped MPA with the modified IBPF. The geometrical parameters of the connecting transmission lines of the antenna and the filter are optimised through numerical simulation in order to match their input impedances with the common reference impedance of 50 Ω. The geometrical parameters of the integrated system are optimized to achieve the desired performance in L-band. The optimized geometrical parameter values of the proposed filtering antenna are given in Table 3.5. The prototype of the proposed filtering antenna was fabricated on RT/duroid 6010 substrate (ε_r = 10.2, tanδ = 0.0023, and thickness = 1.27 mm) using PCB technology for experimental study. Figure 3.11(b) shows top and bottom views of the fabricated prototype of the proposed filtering antenna. The overall physical size of the proposed filtering antenna is 91.8 mm × 47 mm × 1.27 mm.

The input as well as radiation characteristics along with surface current distributions of the proposed antenna with and without the integration of the BPF, are studied through numerical simulation and/or experimentally.

Table 3.5: Optimized geometrical parameter values of the proposed integrated design of filtering antenna (all dimensions are in millimetre)

L = 91.8	W = 47	l_{f1} = 3.5	w_{f1} = 1.7	l_{f2} = 43	w_{f2} = 1.4	l_{g3} = 51	l_{g4} = 51.1
l_c = 3.9	w_c = 3.7	l_t = 2.7	w_t = 4	a_1 = 32.6	a_2 = 7	a_3 = 32.5	b_1 = 6.2
b_2 = 17.4	b_3 = 5.5	l_1 = 19.3	w_1 = 1.8	l_2 = 17.3	w_2 = 1	l_3 = 17.2	w_3 = 2.4
g_{12} = 0.2	g_{23} = 0.3	d_1 = 0.4	d_2 = 0.8	l_4 = 1.6	l_5 = 2.8	l_6 = 2.7	g_1 = 0.7
w_4 = 0.9	l_7 = 0.8	l_8 = 2.6	l_9 = 0.3	g_2 = 0.4	w_5 = 0.4	l_{10} = 3.7	l_{11} = 0.9
l_{12} = 2.5	l_{13} = 1.3	w_6 = 0.2	l_{14} = 8.4	–	–	–	–

3.4.2 Results and Discussion

3.4.2.1 Reflection Coefficient-Frequency Characteristics

Figure 3.12 shows the simulated variations of reflection coefficient with frequency for the proposed antenna with and without integration of the BPF. From Figure 3.12, it can be observed that the proposed integrated design (also called the proposed filtering antenna) provides sharp band-edge selectivity at lower and upper edges of the frequency band (1.01 – 1.96 GHz) along with good suppression of unwanted harmonics up to 8 GHz.

The numerically simulated and measured variations of the reflection coefficient of the proposed filtering antenna with frequency are shown in Figure 3.13. The values of reflection coefficient of the proposed filtering antenna were measured at different frequencies using Anritsu make VNA Master (Model: MS2038C). The simulated (measured) -10 dB reflection coefficient bandwidth of the proposed filtering antenna covers the frequency range 1.01 – 1.96 GHz (1.02 – 1.92 GHz). The simulated and

measured results are nearly in agreement with each other excepting minor variations occurring over the frequency band of interest due to fabrication tolerances and measurement errors.

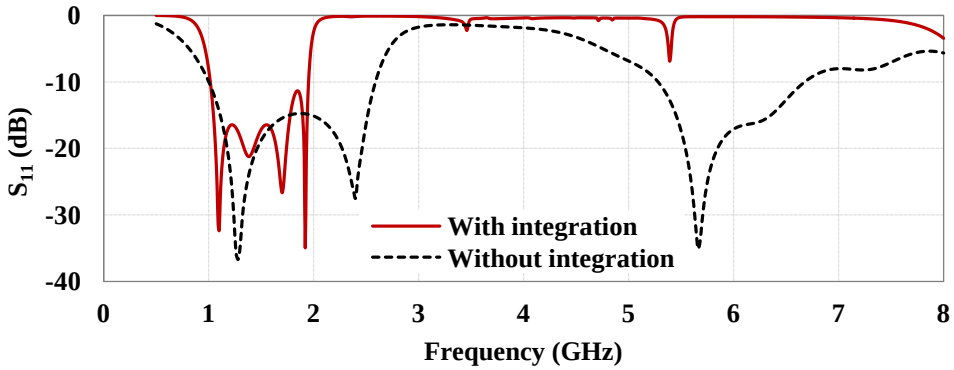

Figure 3.12: Numerically simulated variations of reflection coefficient of the proposed antenna with and without integration of the BPF versus frequency.

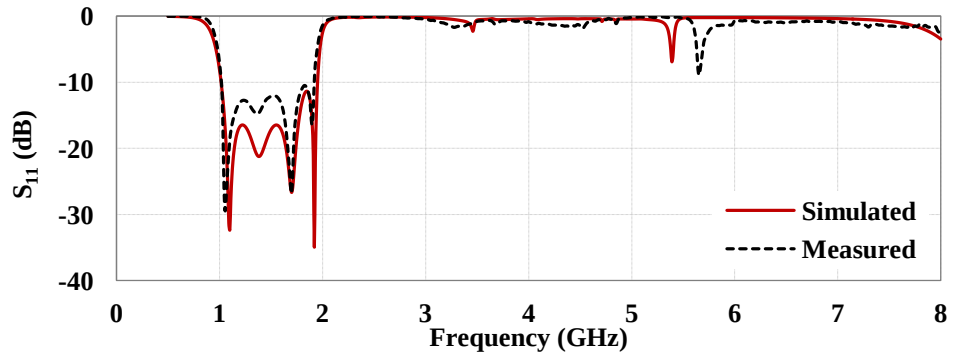

Figure 3.13: Numerically simulated and measured variations of reflection coefficient of the proposed filtering antenna versus frequency.

3.4.2.2 Simulated Surface Current Distributions

For a better understanding of integration effectiveness of the proposed BPF with the proposed antenna for suppression of unwanted harmonics, the current distributions on the surface of the proposed antenna with and without the BPF are studied. Figure 3.14 depicts the current distributions on the surface of the proposed antenna with and without the BPF at a frequency of 5.7 GHz (the frequency at and around which unwanted harmonics without BPF was observed through simulation). It can be noticed from Figure 3.14(a) that a higher level of current reaches the modified elliptic-shaped

radiating patch from the input port in the absence of BPF. Therefore, in order to suppress unwanted harmonics, the BPF was used to block the passage of current from the input port to radiating modified elliptic-shaped antenna. It can be clearly observed from Figure 3.14(b) that in presence of the BPF, the current is more concentrated near the BPF, and negligible current reaches the modified elliptic-shaped antenna at the frequency of 5.7GHz.

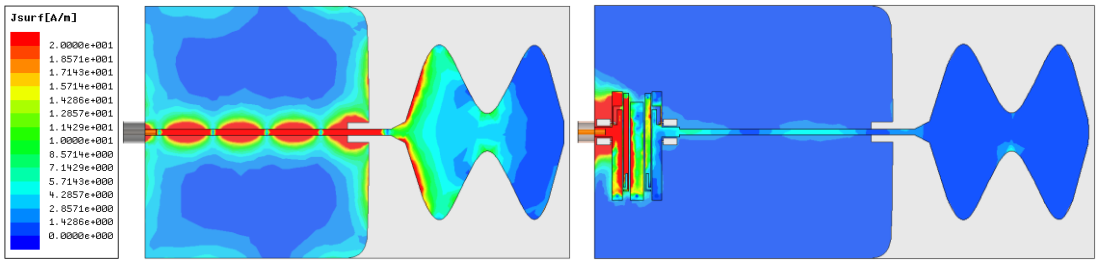

Figure 3.14: Simulated surface current distributions of the proposed antenna at a frequency of 5.7 GHz (an undesired response frequency obtained without BPF) (a) without BPF, and (b) with BPF.

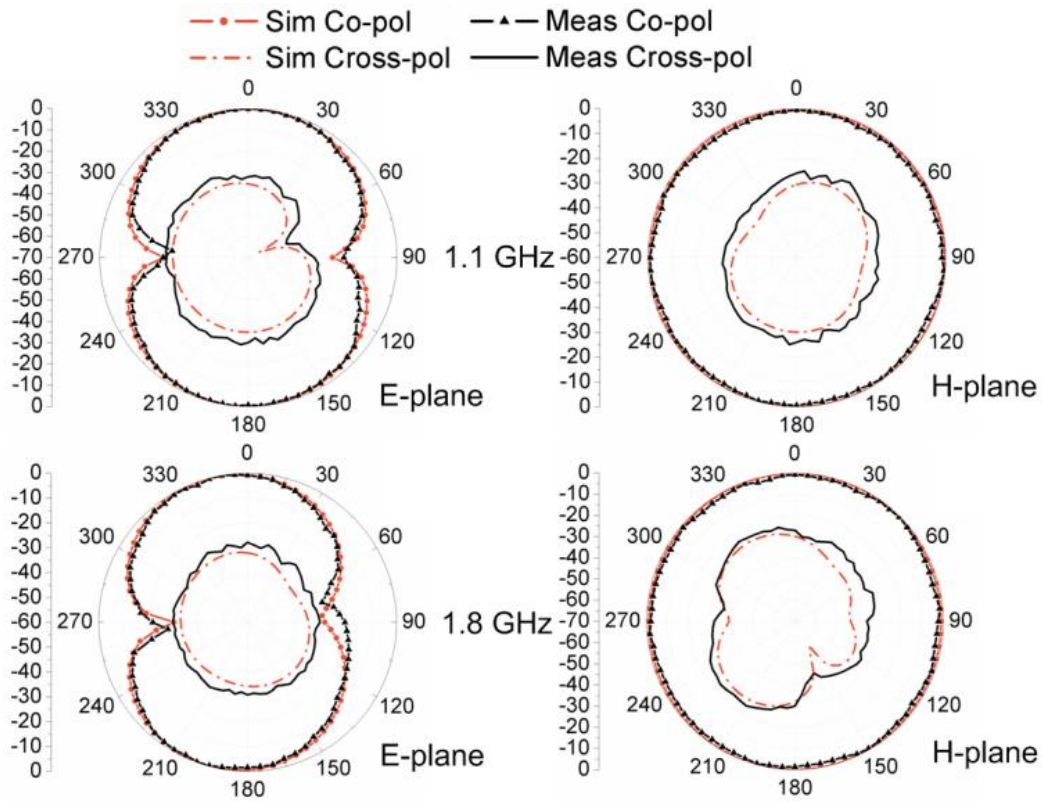

Figure 3.15: Numerically simulated and measured radiation patterns of the proposed filtering antenna for two different frequencies.

3.4.2.3 Radiation Patterns

The simulated and measured co- and cross-polarized radiation pattern plots of the proposed filtering antenna in E- and H-planes for two different frequencies (1.1 and 1.8 GHz) which are within operating frequency band are presented in Figure 3.15. From Figure 3.15, it can be observed that the proposed filtering antenna has good omnidirectional co-polar radiation patterns with low cross-polarization levels at the frequencies considered in the study. The proposed filtering antenna exhibits similar radiation patterns with tolerable cross-polarization levels when compared with the proposed antenna without BPF presented in Figure 3.6 for the same frequencies. It shows that the radiation characteristics of the proposed filtering antenna are more or less maintained with good filtering characteristics over the frequency band of interest.

3.4.2.4 Peak Realized Gain-Frequency Characteristics

Figure 3.16 shows the variations of simulated realized gain values of the proposed antenna with and without integration of the BPF with frequency. From Figure 3.16, it can be observed that the simulated gain values of the proposed filtering antenna vary in the range 1.99 – 2.96 dB within its operating frequency band but drastic reduction in gain values occurs at lower and upper edges of the passband. Though the simulated realized gain values vary in the range 2.1 – 3.5 dB over the passband of the isolated antenna without BPF similar to those for the proposed filtering antenna, not much variation in its gain value occurs beyond the upper edge of the frequency band. The proposed filtering antenna provides simulated lowest and highest realized gain values of -18 dB and -7.5 dB at 2.1 GHz and 5.4 GHz respectively beyond the upper passband edge. In case of the isolated antenna without BPF, simulated realized gain value at 2.1 GHz is 3.1 dB, which is 21.1 dB higher than that for the proposed filtering antenna.

Further, the simulated lowest and highest gain values of the isolated antenna beyond the upper passband edge are found to be -4.1 dB and 4.8 dB at 3.2 GHz and 5.6 GHz respectively. The simulated realized gain value of -18 dB is obtained at 0.85 GHz below the lower passband edge of the proposed filtering antenna. The simulated realized gain value for the isolated antenna without BPF at 0.85 GHz is -4 dB, which is 14 dB higher than that for the proposed filtering antenna. This shows the performance superiority of the proposed filtering antenna over the isolated antenna without BPF in terms of the realized gain parameter.

Figure 3.17 shows the variations of simulated and measured realized gain values of the proposed filtering antenna with frequency. The simulated (measured) realized gain values vary in the range 1.99 – 2.96 dB (1.82 – 2.71 dB) over the operating frequency band 1.01 – 1.96 GHz (1.02 – 1.92 GHz). The simulated and measured realized gain-frequency characteristics of the proposed filtering antenna are nearly in agreement with each other.

3.4.2.5 Simulated Total Efficiency-Frequency Characteristic

Figure 3.18 shows the variations of simulated total efficiency of the proposed antenna with and without integration of the BPF with frequency. From Figure 3.18, it can be observed that the simulated total efficiency of the proposed filtering antenna varies in the range 85 – 89 % within its operating frequency band but drastic reduction in total efficiency occurs on either side of the passband (= 1.01 – 1.96 GHz). The simulated total efficiency values vary in the range 86 – 93 % over the passband of the isolated antenna without BPF similar to those for the proposed filtering antenna. It can be stated after comparing the total efficiency-frequency characteristics of the proposed antenna with and without integration of the BPF that significant suppression in the total

efficiency value occurs above the desired passband in case of proposed filtering antenna i.e. the proposed MPA integrated with the proposed modified IBPF as compared with the isolated antenna without integration of BPF. This shows the performance superiority of the proposed filtering antenna over the isolated antenna without the BPF in terms of total efficiency parameter.

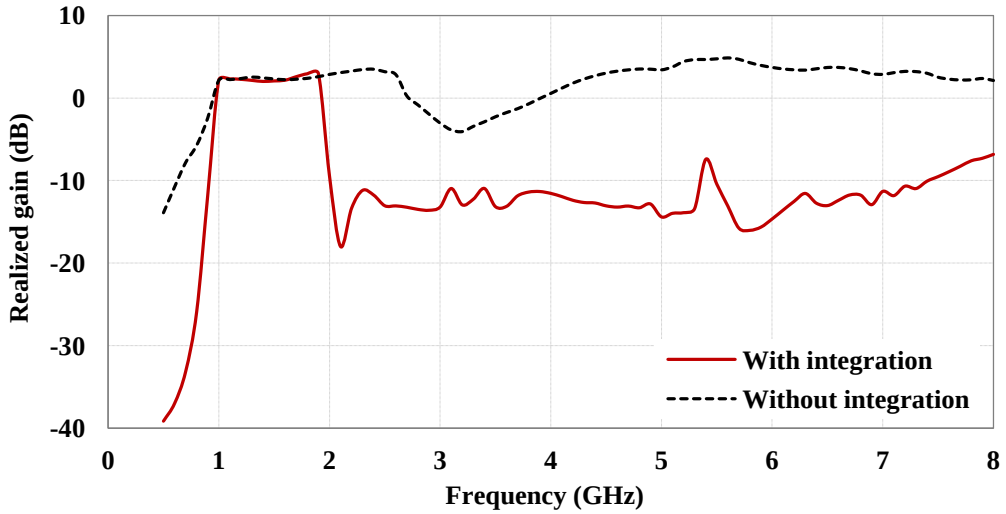

Figure 3.16: Numerically simulated variations of gain values of the proposed antenna with and without integration of the BPF versus frequency.

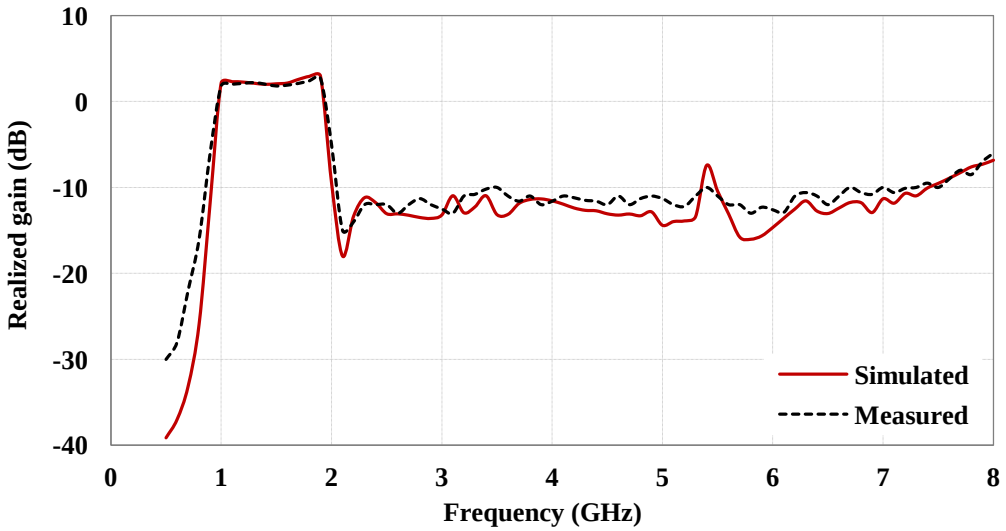

Figure 3.17: Numerically simulated and measured gain values of the proposed filtering antenna as functions of frequency.

3.4.2.6 Performance Comparison of the Proposed Filtering Antenna with Those Reported in Literature

Finally, performance and dimension based comparison of the proposed filtering antenna with those reported in the literature is given in Table 3.6. It is apparent from Table 3.6 that overall electrical size of the proposed filtering antenna (in terms of free space wavelength, λ_l) is smaller as compared with the filtering antennas reported in the literature. The proposed filtering antenna also provides good harmonic suppression capability with improved selectivity.

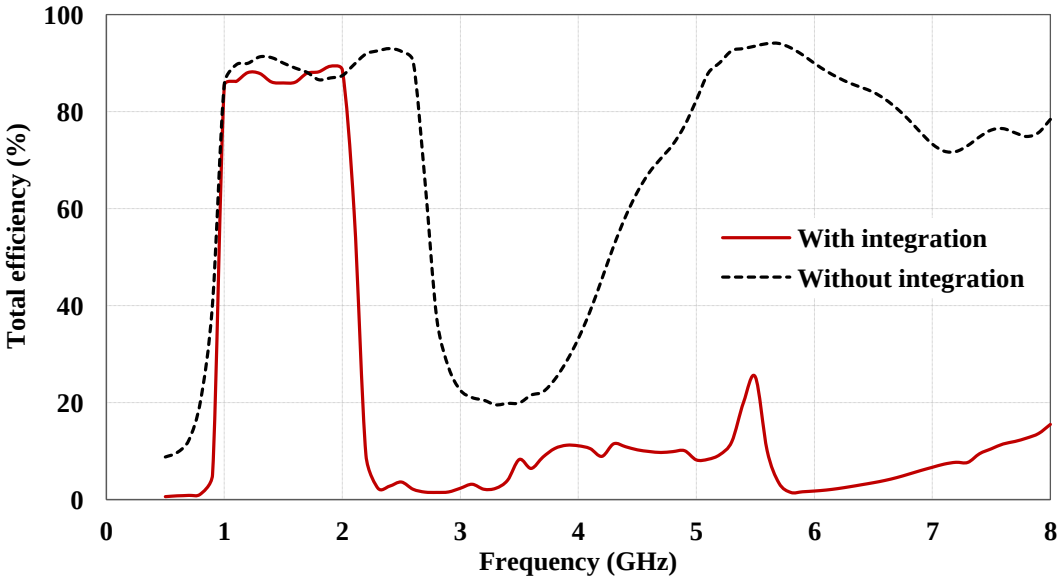

Figure 3.18: Numerically simulated variations of total efficiency of the proposed antenna with and without integration of the proposed BPF versus frequency.

Table 3.6: Performance comparison of the proposed filtering antenna and filtering antennas reported in the literature.

Reference	Measured -10 dB reflection coefficient bandwidth (FBW)	Measured harmonic suppression	Physical size (mm × mm)	Electrical size ($\lambda_l \times \lambda_l$)
[Zuo *et al*. (2009)]	4.06 – 4.26 GHz (4.7%)	Not available	20 × 40	0.27 × 0.54
[Wu *et al*. (2011)]	2.26 – 2.66 (16.3%)	Upto 3.5 GHz	30 × 45	0.226 × 0.339
[Mansour *et al*. (2014)]	1.99 – 2.07 GHz (3.5%)	Not available	85 × 80	0.56 × 0.53
[Cheng and Li (2017)]	2.32 – 2.55 GHz (9.4%)	Upto 3.5 GHz	70 × 75	0.54 × 0.58
Proposed filtering antenna	**1.02 – 1.92 GHz (61.2%)**	**Upto 8 GHz**	**91.8 × 47**	**0.31 × 0.16**

λ_l is the free space wavelength at the lower cut-off frequency (f_l). FBW stands for fractional bandwidth.

3.5 Conclusion

A compact filtering antenna having sharp cut-off performance and reasonably suppressed unwanted harmonics has been described in this chapter. The proposed filtering antenna has been obtained through integration of the proposed modified elliptic-shaped MPA with the modified IBPF presented in chapter 2 and tunning the geometrical parameters for obtaining desired filtering antenna characteristics in L-band. The proposed filtering antenna is compact in size with good band-edge selectivity and reasonably suppressed out-of-band harmonics up to 8 GHz. The proposed filtering antenna and the isolated antenna without BPF have been investigated through numerical simulation and measurements. The simulation results for the proposed filtering antenna and the isolated antenna have been found to be nearly in agreement with the respective experimental ones. It is finally concluded that the proposed compact filtering antenna

can be a good candidate for various L-band wireless communication applications, such as satellite communication, global positioning system, and aircraft surveillance system.

In chapter 4, the description of a new compact ultra-wideband (UWB) BPF is given along with a new DGS-based lowpass filter (LPF). The DGS-based LPF is integrated with UWB BPF for obtaining improved out-of-band performance of the proposed compact UWB BPF.